Periodica Polytechnica Civil Engineering

Post-cyclic Static Behavior of Carbon Short-fiber-reinforced Concrete (CSFRC) Under Tension

Ante Džolan[1*], Željko Smolčić[1], Oliver Fischer[2], Dragan Ćubela[3]

[1] Department for Structural Engineering, Faculty of Civil Engineering, University of Rijeka, Radmile Matejčić 3, 51000 Rijeka, Croatia
[2] Chair of Concrete and Masonry Structures, Technical University of Munich, Theresienstraße 90-Gebäude N6, 80333 Munich, Germany
[3] Department for Mechanics, Materials and Structures, Faculty of Civil Engineering, Architecture, and Geodesy, University of Mostar, Matice hrvatske bb, 88000 Mostar, Bosnia and Herzegovina
[*] Corresponding author, e-mail: ante.dzolan@uniri.hr

Received: 11 December 2025, Accepted: 07 July 2026, Published online: 28 July 2026

Abstract

Ultra-high-performance concrete (UHPC) is of interest to many researchers today. This concrete is produced by adding fibers to the fresh concrete matrix during mixing, where the matrix is a fine-grained mix with a maximum particle size of 1 mm. Various types of fibers can be added to the concrete matrix: steel, natural, polypropylene, polyvinyl alcohol, etc. fibers. Short carbon fibers are also used. Reinforcing concrete with short carbon fibers results in carbon short-fiber-reinforced concrete (CSFRC). CSFRC has approximately twice the tensile strength of high-strength concrete (HSC) and about 400% higher tensile strength than normal-strength concrete. In addition to high tensile strength, CSFRC is also characterized by ductile behavior under tension and flexion. Although this concrete has been the subject of much research, its behavior has not been sufficiently studied yet to be fully explained. Thus, there are no available results on its post-cyclic static behavior in the literature. Therefore, an aim of this work is to provoke further research in this area. To this end, experimental results obtained from two specimens are presented here. In both tests, tensile prior cyclic loading preceded tensile static loading, and the behavior of CSFRC under these loadings is observed. The number of cycles of harmonic loading preceding the static loading varied: one specimen underwent 6 million cycles, and the other 10 million. The results show a difference; the specimen with lower number of cycles failed in an elasto-plastic manner, while the specimen with higher number of cycles failed in a brittle manner.

Keywords

carbon short-fiber-reinforced concrete (CSFRC), cyclic loading, static loading, training effect, strain, linearity, non-linearity

1 Introduction

As a building material, concrete has been used for over two thousand years, dating back to Roman concrete, and for more than 150 years as reinforced concrete. During this time, it has been suffered significant transformations in order to enhance its mechanical properties. Today, it is commonly used as reinforced concrete (RC) or prestressed concrete (PC). In these types, the tensile mechanical properties of concrete are improved by adding steel reinforcement bars and/or steel tendons in regions where the highest tensile stress is expected. It can be conditionally said that, in this way, concrete is reinforced at the "macro level". However, a major focus of current research is on concrete that is reinforced at the "micro level". Through micro-reinforcement, the mechanical properties of concrete are improved at countless points within the concrete matrix, meaning the improvement is not limited only to regions where the highest tensile stress is expected. Micro-reinforcement of concrete is achieved by incorporating different types of fibers into the fresh concrete matrix [1–19]. Any type of fibers improves the concrete tensile strength. As shown in [1], concrete reinforced with steel fibers has 40% higher tensile strength than reference plain concrete, while reinforcing concrete with glass fibers increases its tensile strength by 18% [18]. In a concrete matrix reinforced with polyvinyl alcohol fibers, the tensile strength is 52% higher than in reference plain concrete [5]. A concrete matrix reinforced with banana fibers has 47% higher tensile strength than reference plain concrete [3]. Reinforcing concrete with carbon fibers (CF) increases its tensile strength by 65% [4]. It is also possible to combine different types of fibers in the same concrete matrix, so the addition of synthetic

Cite this article as: Džolan, A., Smolčić, Ž., Fischer, O., Ćubela, D. "Post-cyclic Static Behavior of Carbon Short-fiber-Reinforced Concrete (CSFRC) Under Tension", Periodica Polytechnica Civil Engineering, 2026. https://doi.org/10.3311/PPci.43059

discontinuous propylene fibers to a carbon fiber-reinforced concrete matrix slightly improves its adhesion strength [20]. From the findings in the previously provided literature, it is clear that careful attention must be paid to selecting optimal fiber dosage. A high percentage of fibers leads to over-reinforcement of concrete, while a low percentage does not improve concrete properties optimally. In [21, 22], the high-performance concrete matrix is reinforced with 1 vol% short CF, and its tensile strength is about 15 MPa in specimens tested at the age of 28 days, which is approximately 100% higher than that of plain ultra-high-performance concrete. This more significant increase in tensile strength in [21, 22] compared to the previously mentioned references is a result of the method used to build the specimens. Namely, specimens tested in [21, 22] were 3D printed [23–25] so that there is a good angle alignment between the direction of tensile stress and the incorporated fibers; as a matter of fact, the deviation in the angle between the carbon fibers and the tensile stress remained primarily within the range of ±10o [26]. In contrast, in previously analyzed references, the fibers were randomly distributed in the concrete matrix, so not all incorporated fibers were aligned with the tensile stress direction, and their positive influence on the improvement of tensile strength was absent. From the results presented in [21, 22], it is also clear that carbon short-fiber-reinforced concrete (CSFRC) exhibits highly ductile behavior in tension, unlike plain concrete.

In [27], the same concrete matrix like in [21, 22] was used to have analyzed the fatigue behavior of CSFRC under tension and flexion. For the fatigue analysis, a harmonic cyclic load was applied using four different loading procedures. The results showed that an upper harmonic load with a lower upper load level, followed by one with a higher upper load level, contributed to better fatigue behavior in CSFRC compared to a harmonic load with only a higher upper load level from the very beginning of the test. This indicates the possible existence of a training effect in CSFRC. If a training effect does exist in CSFRC, it does not only influence its fatigue behavior but could also have a negative or positive effect (depending on the number of loading cycles) on its mechanical properties after cyclic loading stops.

There is no literature addressing the influence of cyclic loading on the static behavior of CSFRC after the cyclic load stops, actually, on its mechanical properties. Thus, the main aim of this work is to initiate discussion on this topic. Namely, in this study, the results of two static tests, each preceded by cyclic loading, are presented. Since only two static tests were conducted, with a different number of cycles having preceded the static tests, their results can indicate the existence of this influence and provoke further research for its full clarification.

2 Material and methods

2.1 Raw materials and mixing procedure

The CF used to reinforce the concrete matrix were uniformly cut to a length of 3 mm with the following properties: diameter 7 µm, tensile strength 4137 MPa, elasticity modulus 242 GPa, and ultimate tensile strain 1.5%. Before incorporation into the matrix, CF were heat treated as described in [21, 22, 27], and the necessity of this process is discussed in [28]. The influence of CF dosage on the workability of the concrete matrix is provided in [29, 30]. Ensuring the workability of the CSFRC matrix is especially important because the testing specimens were built using 3D printer. All other raw materials are listed in Table 1.

The influences of the superplasticizer and silica fume on the properties of the CSFRC matrix are described in [31, 32] and [28, 33], respectively.

The mixing process is also described in [21, 22, 27], along with the printing process and curing procedure.

2.2 Testing procedure

2.2.1 Preparation of specimens for testing and their installation in testing device

After having been built and cured, the specimens were equipped with measurement sensors and installed in a testing device at the age of 27 days. For measurement of strains, four strain gauges aligned with the direction of the tensile load were glued to the back surface of the specimens at the positions shown in Fig. 1(a) to Fig. 1(c), Light-beam micrometer (LBM) pins were also glued to both sides of the specimens to measure strains at the level of the testing area (Fig. 1(c)). In addition to the strain gauges and LBM, the development of strains (i.e., damage) in the specimens was also analyzed using digital image correlation (DIC), and the opposite (front) surface of the specimens was prepared to this end (Fig. 1(d)).

Table 1 List of raw materials

Component	Type of component	wt%
Cement	Holcim Sulfo 52.5 R	34.70
Silica fume	Sika Silicol P	21.70
Quartz powder	SF 500	21.70
Quartz sand	H33	7.70
Water	–	11.70
Superplasticizer	BASF ACE 460	2.50
Carbon fibers	Zoltek (Toray) PX35, 3 mm	1.00 (vol%)

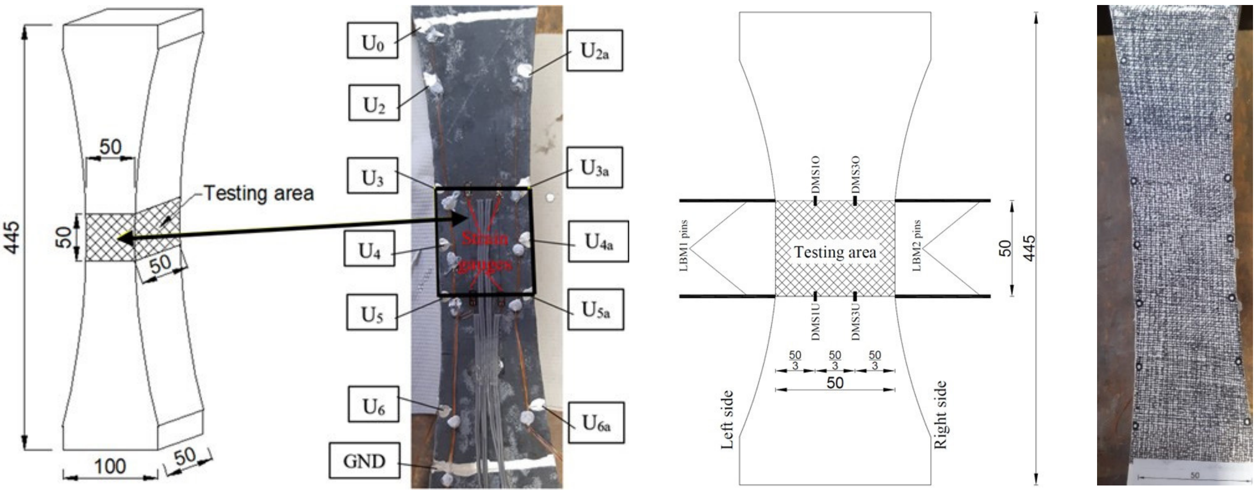

(a) (b) (c) (d)

Fig. 1 View of the geometry of the tested specimens and the installed testing equipment: (a) shape and dimensions of the specimens; (b) specimen surface with installed strain gauges and copper wires for measuring voltage; (c) schematic representation of the positions of the strain gauges and LBM pins [21]; (d) specimen surface prepared for DIC [27]. All measurement units are in mm.

The development of damaging processes in specimens is also analyzed by measuring voltage in the specimens during testing. For this purpose, twenty copper wires were installed on the specimens: five on each edge of the surface with strain gauges (U2-U6, and U2a-U6a, Fig. 1(b)), and five on each side of the specimens near the DIC surface. A more detailed description of this method can be found in [27, 34].

After having been equipped with sensors, the specimens were installed in the testing device using two-component glue. The glue should have been dried for about 24 hours, and then the tests began. Both tests started at the age of 28 days.

2.2.2 Conduction of the tests

During cyclic loading, the harmonic load frequency was 10 Hz, and load-controlled loading was applied. The results were captured by all previously mentioned sensors. DIC images were captured before the start of the harmonic load and every 10 thousand cycles during cyclic loading. In both tests, the upper/bottom load level was set at 80/40% of the tensile strength of CSFRC for the first 3 million cycles, then reduced to 60/20% of the tensile strength for the next 2 million cycles. After these 5 million cycles, the upper/bottom load level was reduced to 40/10% of tensile strength for the first specimen (SNE4.23.3) for about 5 million cycles, and for about 1 million cycles for the second specimen (SNE5.23.3). The CSFRC matrix used in [22] is the same as in this work, so the tensile strength of CSFRC is taken from that source (15 MPa). The cyclic tests were stopped after these 10 million and 6 million cycles, respectively. Afterwards, all sensors were reset to zero, and the static tests were conducted. During static tests following the cyclic loading, the specimens were subjected to a short-term static tensile load in a displacement-controlled manner. The loading rate was set to 0.003 mm/s, and the load increased until the specimens broke. The behavior of specimens during the tests was recorded by all mentioned sensors.

3 Results

3.1 Behavior during harmonic load

The previously mentioned test names (SNE4.23.3 and SNE5.23.3) refer to the static tests conducted after the cyclic load was stopped. Results for these cyclic tests under harmonic load were already published in [27], where the test names were E4.23.3 and E5.23.3.

The cyclic (i.e., fatigue) behavior of these specimens was described in detail in [27], and, since it precedes the static tests, only a brief description of this behavior is provided here, as well as additional observations that were not noted in [27].

Based on the strain development during cyclic loading shown in Fig. 2, it is clear that the specimens are in a state of global non-linearity from the very beginning of the application of the harmonic load [27]. Although test E4.23.3 was stopped after about 10 million cycles, the results presented in Fig. 2(a) are given for 6 million cycles. Afterwards, there are no significant changes in the results, and so at the time the test was stopped, the measured strains were: DMS1U – 1.33‰, DMS1O – 0.182‰, DMS3O – 0.704‰, and DMS3U – 2.13‰. The lack of convergence in the results of these two specimens is due to the fact that the specimens are in a state of global non-linearity, so the strain gauges can be closer to or farther from the position of cracks.

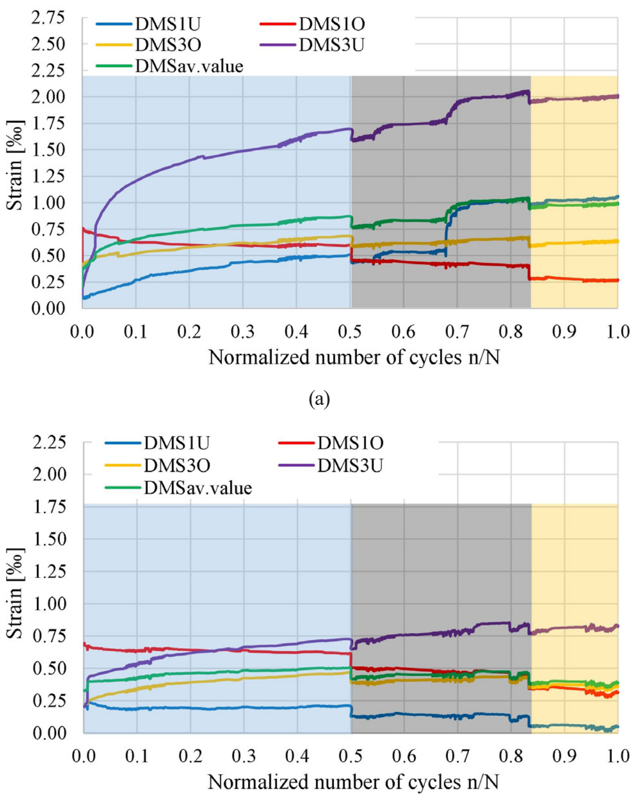

Fig. 2 Strain development during cyclic loading obtained using strain gauges: (a) for the test E4.23.3 [27]; (b) for the test E5.23.3. N = 6 million cycles.

The results shown in Fig. 2 are also confirmed by those obtained using DIC (Fig. 3). Fig. 3(a) and Fig. 3(e) confirm the results from Fig. 2; both specimens are in a state of global non-linearity before the application of harmonic load. Namely, before the start of cyclic loading, the load was increased from 0 to 80% of the tensile strength in a static manner, then reduced to the average value between the upper and bottom load levels (Fig. 3(a) and Fig. 3(e) correspond to this moment), and only after that, the cyclic loading began. In the next 3 million cycles (Fig. 3(b) and Fig. 3(f)), new cracks are opened and existing cracks are propagated. After a reduction in the harmonic load, during the following 2 million cycles, some cracks are closed and others are narrowed (Fig. 3(c) and Fig. 3(g)). Further cracks' closing and narrowing are observed in Fig. 3(d) and Fig. 3(h) after the cyclic load was reduced again, actually, at the time when the tests were stopped. However, more fully opened cracks are observed in specimen E5.23.3 (Fig. 3(h)) than in specimen E4.23.3 (Fig. 3(d)). This is a consequence of material fatigue. Namely, specimen E4.23.3 was subjected to a higher number of harmonic load cycles, and due to material fatigue, many microcracks were opened, causing a relaxation of previously fully opened cracks. As a result, the damage and energy dissipation capacity of the specimen was reduced.

All these findings correspond with the change in voltage in the specimens during the cyclic tests, which is analyzed in [27].

3.2 Post-cyclic static behavior

The condition of the specimens (cracks and damage) described in Section 3.1 is actually the initial state of the specimens for the static tests. Since this condition represents the zero state for the static tests, it does not appear in the results obtained from the static tests.

3.2.1 Stress-strain diagrams

The results obtained by strain gauges for specimen SNE4.23.3 are given in Fig. 4(a). These results demonstrate linear behavior at the location of each strain gauge. However, the lack of alignment among these results (i.e., lines) indicates a global non-linearity in the testing area, that is in the specimen. Thus, although there is global non-linearity in the specimens due to prior cyclic loading, there is local linearity at the strain gauge positions during static loading. Since the results clearly show that there is no local non-linearity during static tests, it is evident that the ductility and damage (i.e., energy dissipation) capacity of the specimens were expended during cyclic loading. As a result, the failure of the specimen in the static test is brittle. In Fig. 4(a), an average line derived from the four strain gauges is formed representing the behavior of the entire testing area. Comparing this average line with the results obtained by LBM (Fig. 4(b)) shows that the average line reliably represents the behavior of the entire testing area. From the diagrams in Fig. 4, it can be read that the tensile strength of the specimen is 12 MPa. Comparing this value with that presented in [22] (15 MPa), it is evident that prior cyclic loading reduced the tensile strength by 20%.

The analog results are shown in Fig. 5 for specimen SNE5.23.3. Analyzing the results from all four strain gauges (Fig. 5(a)), it is evident that the results from strain gauge DMS1O don't match those from the other three gauges. This fact indicates global non-linearity of the specimen. However, unlike specimen SNE4.23.3, the results from the other three strain gauges in specimen SNE5.23.3 show very good alignment. Hence, although global non-linearity exists in specimen SNE5.23.3, its ductility and damage (i.e., energy dissipation) capacity were not fully expended during prior cyclic loading. This is confirmed by the existence of the yielding region in Fig. 5(a).

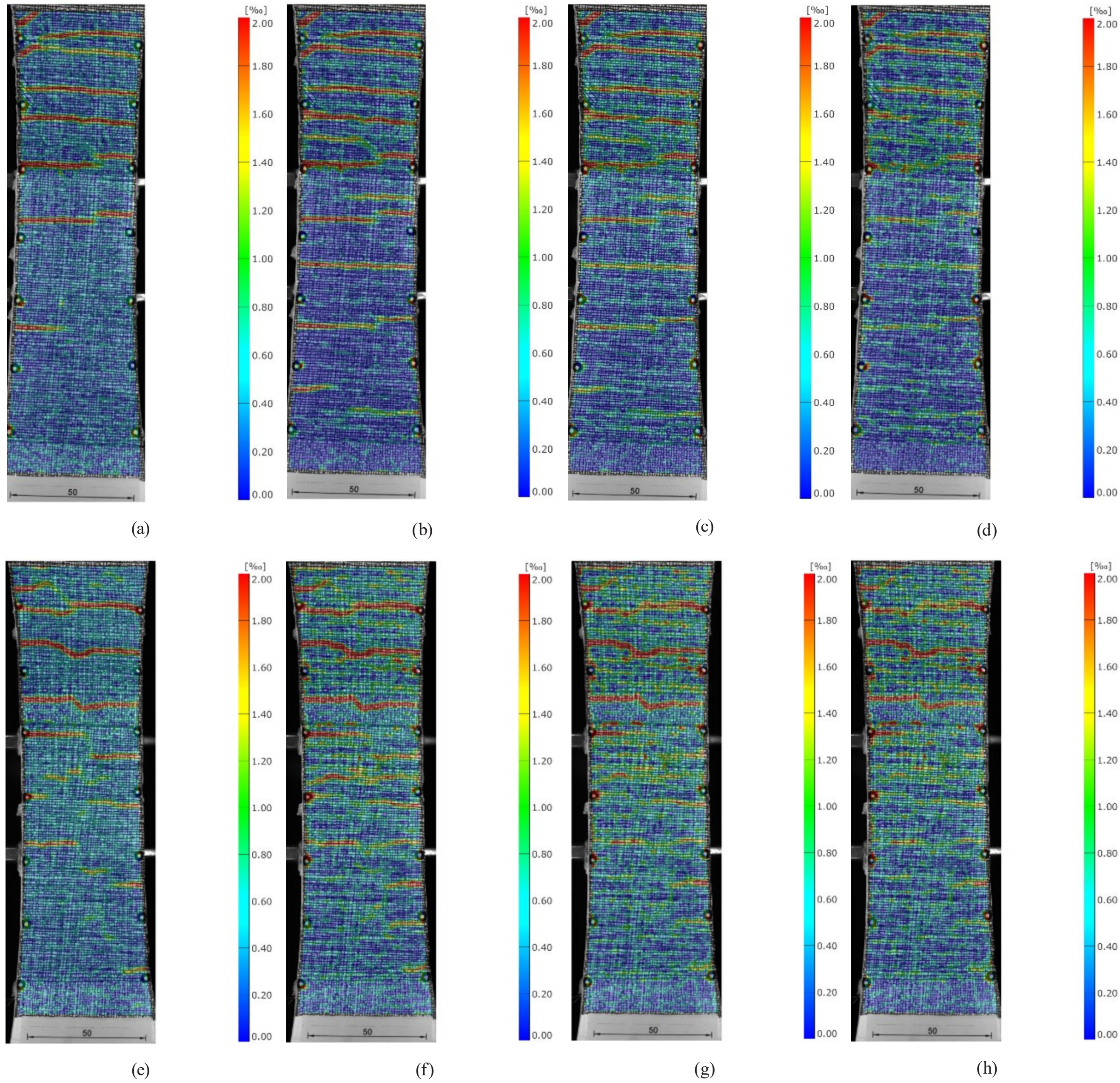

Fig. 3 View of the strain state in specimen E4.23.3: (a) immediately before the start of cyclic loading; (b) after 3 million cycles; (c) after 5 million cycles; (d) after cyclic test was stopped – 10 million cycles; and view of the strain state in specimen E5.23.3: (e) immediately before the start of cyclic loading; (f) after 3 million cycles; (g) after 5 million cycles; (h) after cyclic load test was stopped – 6 million cycles.

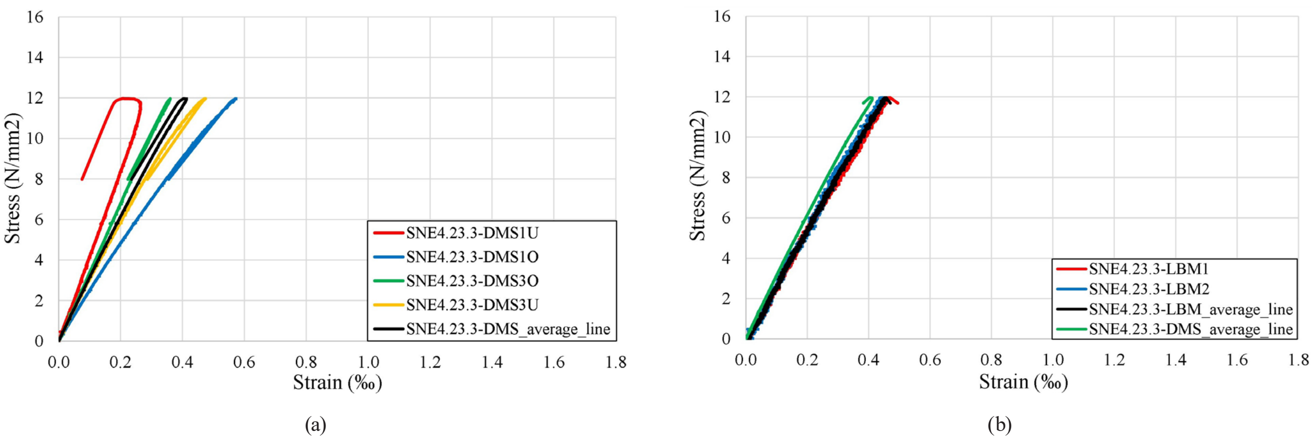

Fig. 4 Stress-strain diagram for specimen SNE4.23.3: (a) obtained by strain gauges; (b) LBM

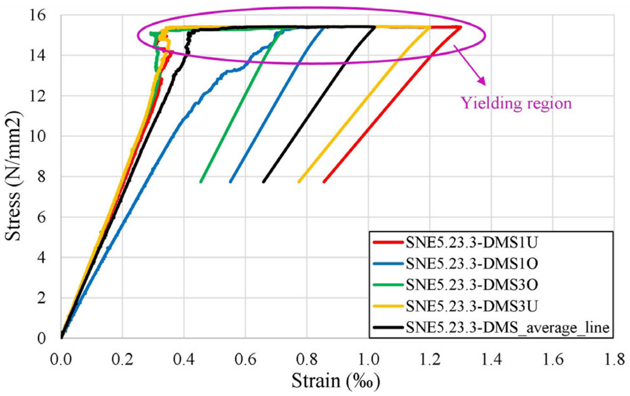

(a)

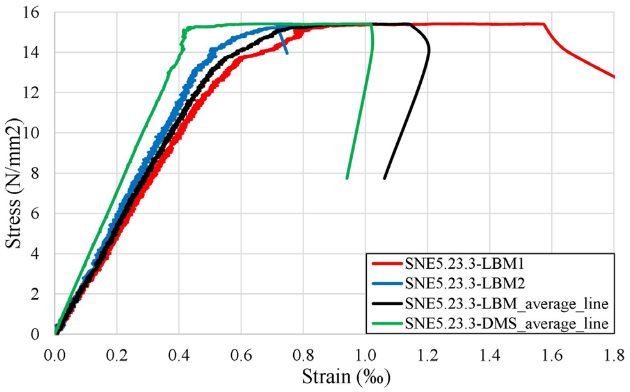

(b)

Fig. 5 Stress-strain diagram for specimen SNE5.23.3: (a) obtained by strain gauges; (b) LBM (b)

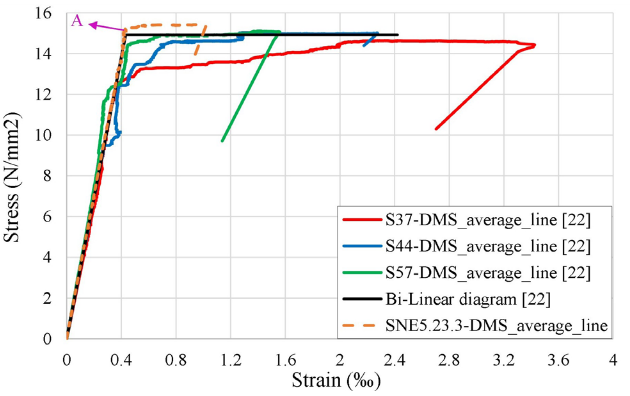

Fig. 6 Comparison of the average DMS line (stress-strain diagram) of specimen SNE5.23.3 with results published in [22].

The presence of the yielding region confirms that new cracks are opened, which were not present during cyclic loading. The average line from all four strain gauges is derived (Fig. 5(a)), and this line is compared with the results published in [22] in Fig. 6, corresponding to specimens loaded at the age of 28 days. From Fig. 6, it is evident that prior cyclic loading contributes to a slight increase in tensile strength. Thus, the tensile strength of specimen SNE5.23.3 is 15.40 MPa (Fig. 5 and Fig. 6), while the average strength of the specimens in [22] is about 15 MPa. Accordingly, the tensile strength increases by 2.7% due to prior cyclic loading. However, this tensile strength may also be attributed to the stochastic behavior of the material, and the actual cause should be determined by further research. Unlike tensile strength, prior cyclic loading negatively influences ductility, i.e., ultimate tensile strain. In the specimens in [22], the average ultimate strain is 2.42‰, while it is 1.02‰ in specimen SNE5.23.3, representing a decrease of 57.85%. The behavior of specimen SNE5.23.3 shows good agreement with the behavior of the specimens from [22] in the linear region (Fig.6). However, when the average DMS line of specimen SNE5.23.3 is compared with LBM results (Fig. 5(b)), it is clear that it underestimates the damage of the specimen due to prior cyclic loading. This can be due to a possibility that strain gauges DMS1U, DMS3O, and DMS3U were close to the opened cracks and the strains at their locations were relaxed.

3.2.2 DIC results

The results obtained using DIC for specimens SNE4.23.3 and SNE 5.23.3 immediately before failure are shown in Fig. 7(a) and Fig. 7(c), respectively, and the locations of the main cracks that caused their failure are given in Fig. 7(b) and Fig. 7(d), respectively.

Comparing Fig. 7(a) and Fig. 7(c), more intense strains - actually cracks – are visible in specimen SNE5.23.3 than in specimen SNE4.23.3. This confirms the results shown in Figs. 4 and 5, that is the damage capacity of specimen SNE4.23.3 was expended during prior cyclic loading, so no new cracks appear in static test, resulting in brittle failure of the specimen. This is also confirmed by comparing Fig. 7(a) and Fig. 7(b). It is evident that there was no open crack at the position where the specimen broke (Fig. 7(a) and Fig. 7(b)). However, comparing the position of the main crack in Fig. 7(b) with the state of cracks during cyclic loading (Figs. 3(a)–(d)), it is clear that this crack was opened during cyclic loading and was not recorded during static loading because all cracks recorded during cyclic loading were reset to zero at the start of the static test. This does mean that this crack was not even widened during the static test because its energy dissipation capacity was expended during prior cyclic loading.

More pronounced cracks in Fig. 7(c) indicate that the cracks opened during prior cyclic tests (Figs. 3(e)–(h)) widened in the static test; however, comparing the cracks in Fig. 7(c) with those in Figs. 3(e)–(f) shows that new cracks appeared during the static test too. These observations confirm the results obtained using strain gauges:

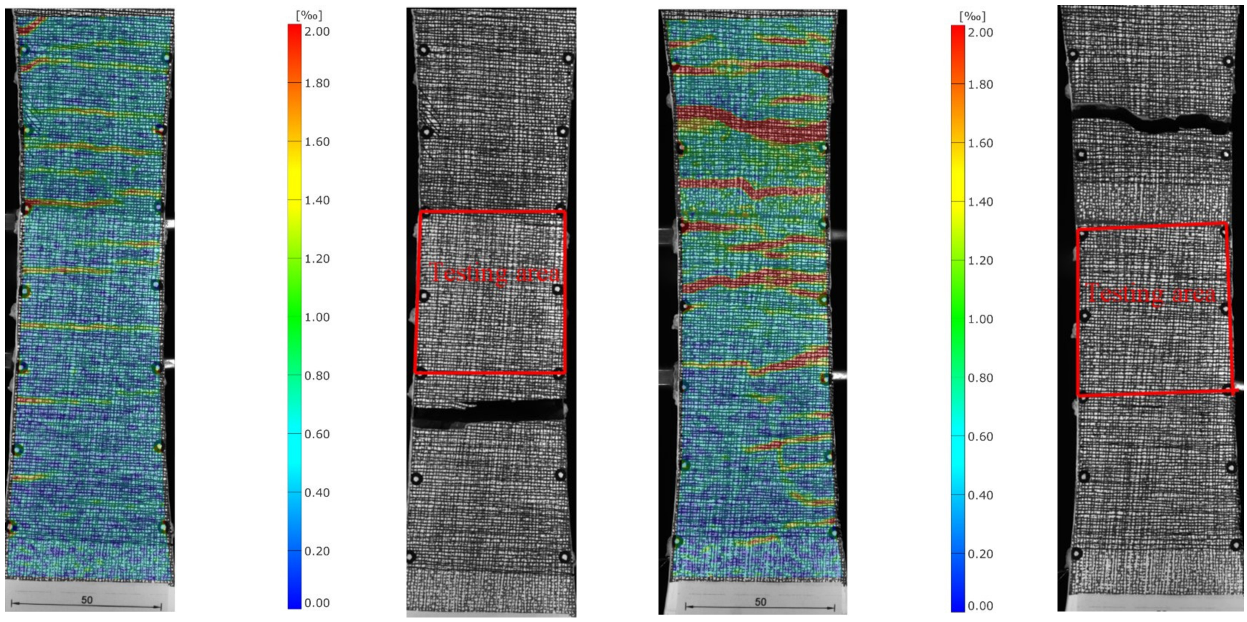

(a) (b) (c) (d)

Fig. 7 DIC results and positions of the main cracks: (a) DIC results for specimen SNE4.23.3 immediately before failure; (b) position of the main crack in specimen SNE4.23.3; (c) DIC results for specimen SNE5.23.3 immediately before failure; (d) position of the main crack in specimen SNE5.23.3.

the ductility and damage (energy) dissipation capacity of the specimen was not expended during prior cyclic loading, nor was the energy dissipation capacity of the cracks opened during prior cyclic loading. The crack causing the failure of specimen (Fig. 7(d)) is visible immediately before failure in Fig. 7(c), indicating the failure was announced.

From Fig. 7(b) and Fig. 7(d), it is clear that the failure of both specimens occurred outside the testing area. In contrast, the failure of the specimens from [22], mentioned in Fig. 6, occurred inside the testing area. This indicates that prior cyclic loading increased the energy dissipation capacity in the testing area of specimens subjected to cyclic loading compared with those that the cyclic loading did not precede to.

3.2.3 Measuring of the voltage

Normalized voltage in electrodes in specimens SNE4.23.3 and SNE5.23.3 are shown in Fig. 8(a) and Fig. 8(b), respectively. It is clear that there is no increase in voltage during the static test SNE4.23.3 until the specimen broke (Fig. 8(a)). This means that the cracks opened during prior cyclic loading are not widened during the static tests, and no new cracks appear too. These results fully confirm those obtained with other measuring sensors.

An analog analysis of normalized voltage in specimen SNE5.23.3 can be performed either (Fig. 8(b)). Unfortunately, electrode U2c was broken during preparation of the static test, so there are no results for it. From the results in Fig. 8(b), no change in voltage occurs until the stress reaches about 9 MPa. Afterwards, an increase in voltage is observed, indicating the widening of cracks opened during prior cyclic loading and the appearance of new cracks.

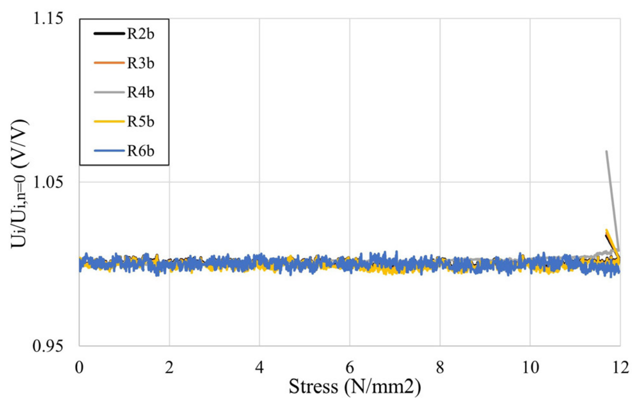

(a)

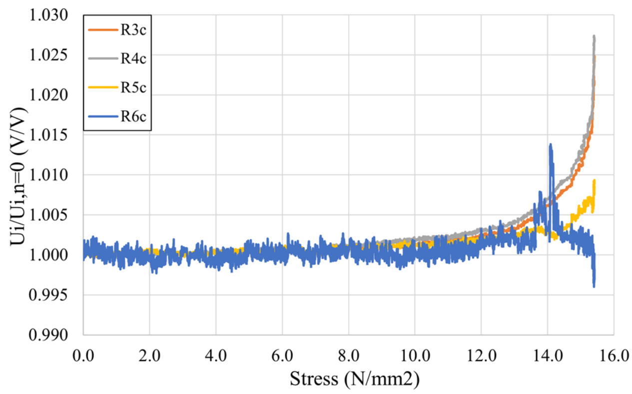

(b)

Fig. 8 Normalized voltage: (a) in specimen SNE4.23.3; (b) in specimen SNE 5.23.3.

Voltage increases more significantly at electrodes U3c and U4c, indicating more significant damage propagation at these positions than at the positions of the other two electrodes. This is evident when these results are compared with those in Fig. 7(c). These results also confirm those obtained by strain gauges and LBM.

3.2.4 Total behavior of CSFRC under post-cyclic static loading

From the previous description of results, it is evident that the results obtained during cyclic loading and static loading can be observed independently. However, this approach leads to incorrect conclusions about the total behavior of CSFRC under post-cyclic static loading. Namely, making decisions about CSFRC behavior under post-cyclic static loading based on the average lines shown in Figs. 4 and 5 leads to the conclusion that the behavior of specimen SNE4.23.3 is linear, followed by brittle failure, while the behavior of specimen SNE5.23.3 is a combination of linear and yielding parts characterized by ductility. Thus, post-cyclic loading behavior can be either linear or non-linear (Fig. 9(a)). However, CSFRC behavior during cyclic loading can also be linear or non-linear (Fig. 9(a)), and this behavior precedes the static behavior. Therefore, conclusions about the total behavior can only be drawn if it is considered as a combination of behavior during both cyclic and static loading. Bearing this in mind, it is clear that in both tests the total behavior is non-linear that is also confirmed by the disagreement of results from different strain gauges. The same conclusion can be drawn when the elasticity modulus of the average line given in Fig. 4(a) (29.10 GPa for SNE4.23.3) is compared with the average elasticity modulus obtained in [22] (34.55 GPa). The same applies to specimen SNE5.23.3 if its elasticity modulus calculated from the average line obtained using LBM (Fig. 5(b)) (26.10 GPa) is compared with the elasticity modulus calculated in [22].

A mistake occurs if a conclusion about total behavior is drawn solely from the results of static loading, as schematically presented in Fig. 9(b) for strain consideration. Thus, the total strain is the sum of the strain reached during cyclic loading and the strain reached during static loading. Neglecting strain developed during cyclic loading, the total strain is equal to that reached during static loading.

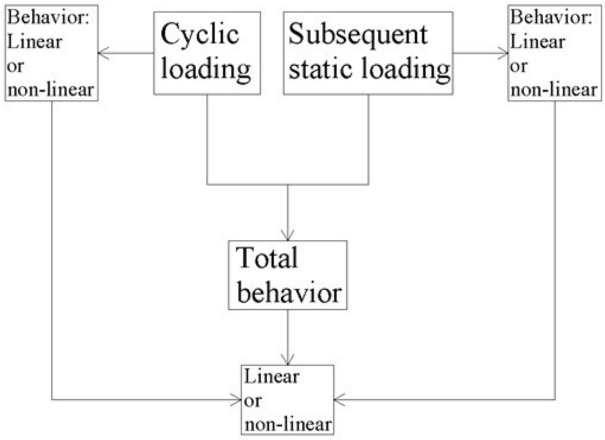

(a)

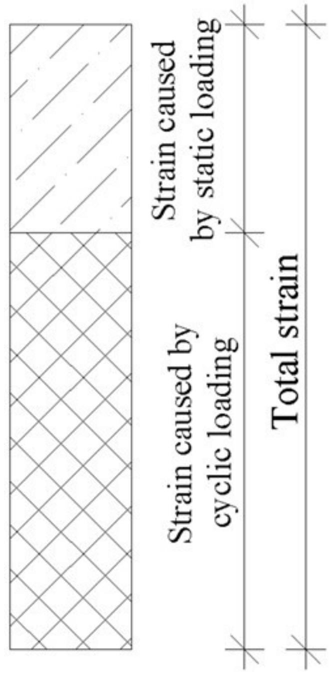

(b)

Fig. 9 Schematic view of the CSFRC behavior: (a) overall behavior under post-cyclic static loading; (b) schematic view of strain under cyclic and subsequent static loading.

4 Conclusions

Based on the analysis above, the next conclusions are drawn:

- The post-cyclic static behavior of CSFRC is significantly influenced by prior cyclic loading.
- The greater the number of cycles of the harmonic load, the worse the post-cyclic static behavior, and *vice versa*. Consequently, the failure varies from brittle to elasto-plastic, depending on the number of cycles preceding the static tests.
- In specimen SNE5.23.3, the number of cycles was about 6 million, which is considered a high number of cycles. However, in spite of this, CSFRC ductility was not expended during cyclic loading. Therefore, it would be interesting to observe the effect of an even lower number of cycles on the post-cyclic static behavior.
- In both tests, the upper load level was 80% of the tensile strength, causing cracks to appear before the start of the harmonic load. It would be interesting to observe what the post-cyclic static behavior would be if a cyclic load with lower upper load level preceded the static loading.

- The achieved state of strains, damage, etc. of CSFRC developed during cyclic loading must be neglect during analysis of post-cyclic static behavior by no means.
- As the influence of prior cyclic loading on post-cyclic static behavior depends on the number of cycles and the magnitude of the bottom/upper harmonic load level, further research should be conducted to confirm or deny the possibility of a training effect in CSFRC.
- The presented results show that specimen SNE5.23.3 is "relatively well trained", while specimen SNE4.23.3 is "overtrained."

Acknowledgments
This research was funded by the German Research Foundation (DFG) as part of the Priority Program SPP2020: "Cyclic deterioration of High-Performance Concrete in an experimental-virtual lab" (Grant Numbers FI1720/7-1, GR1664/13-1, PE1464/6-1, VO829/13-1). The researchers also express their gratitude to everyone involved in the priority program SPP2020, as the working atmosphere between the groups is created by fruitful collaboration.

References

[1] Ammeri, A., Neifar, M. "High Strength Fiber Reinforced Concrete with Local Materials", International Journal of Engineering Research and Technology, 8(10), pp. 403–406, 2019. https://doi.org./10.17577/IJERTV8IS100153

[2] Brandt, A. M. "Fibre reinforced cement-based (FRC) composites after over 40 years of development in building and civil engineering", Composite Structures, 86(1), pp. 3–9, 2008. https://doi.org/10.1016/j.compstruct.2008.03.006

[3] Chandre Mouli, K., Anitha, V., Sree Naga Chaitanya, J. "Comparative Study of Banana fibre Reinforced Concrete with Normal concrete", [online] SSRG International Journal of Thermal Engineering, Special issue, pp. 73–76, 2018. Available at: https://www.internationaljournalssrg.org/uploads/specialissuepdf/ICITSET/2018/TE/IJTE-ICITSET-P102.pdf [Accessed: 01 December 2025]

[4] Chen, Z. Y., Yang, J. "Experimental Study on Dynamic Splitting Characteristics of Carbon Fiber Reinforced Concrete", Matereals, 14(1), 94, 2021. https://doi.org/10.3390/ma14010094

[5] Devi, M., Kannan, L., Ganeshkumar, M., Venkatachalam, T. S. "Flexural Behavior of Polyvinyl Alcohol Fiber Reinforced Concrete", SSRG International Journal of Civil Engineering, 4(6), pp. 27–30, 2017. https://doi.org/10.14445/23488352/IJCE-V4I6P104

[6] Guo, X., Xiong, G. "Resistance of fiber-reinforced fly ash-steel slag based geopolymer mortar to sulfate attack and drying-wetting cycles", Construction and Building Materials, 269, 121326, 2021. https://doi.org/10.1016/j.conbuildmat.2020.121326

[7] Hamad, H. M., Shi, J., Al Jawahery, M. S., Majdi, A., Yousif, S. T., Kaplan, G. "Application of natural fibers in cement concrete: A critical review", Materials Today Communications, 35, 105833, 2023. https://doi.org/10.1016/j.mtcomm.2023.105833

[8] Hannawi, K., Bian, H., Prince-Agbodjan, W., Raghavan, B. "Effect of different types of fibers on the microstructure and the mechanical behavior of Ultra-High Performance Fiber-Reinforced Concretes", Composites Part B: Engineering, 86, pp. 214–220, 2016. https://doi.org/10.1016/j.compositesb.2015.09.059

[9] Insaurriaga, G. L., Gomes, C. C., Ribeiro, F. V., Calegaro, G. L., Silveira, T. A., Cruz, L. F., Cruz, J. A., Amico, S. C., Delucis, R. A. "Effect of Nybridization of Carbon Fibers on Mechanical Properties of Cellulose Fiber-Cement Composites: A Response Surface Methodology Study", C Journal of Carbon Research, 10(2), 41, 2024. https://doi.org/10.3390/c10020041

[10] Kosmatka, S. H., Panarese, W. C., Kerkhoff, B. "Design and Control of Concrete Mixtures – The guide to applications methods, and materials", [online] Portland Cement Association, 2011. ISBN 0-89312-272-6 Available at: Available at: https://secement.org/wp-content/uploads/2019/01/eb001.15.pdf [Accessed: 01 December 2025]

[11] Larsen, I. L., Thorstensen, R. T. "The influence of steel fibres on compressive and tensile strength of ultra high performance concrete: A review", Construction and Building Materials, 256, 119459, 2020. https://doi.org/10.1016/J.CONBUILDMAT.2020.119459

[12] Liu, J., Lv, C. "Durability of Cellulosic-Fiber-Reinforced Geopolymers: A Review", Molecules, 27(3), 796, 2022. https://doi.org/10.3390/molecules27030796

[13] Liu, J., Lv, C. "Properties of 3D-Printed Polymer Fiber-Reinforced Mortars: A Review", Polymers, 14(7), 1315, 2022. https://doi.org/10.3390/polym14071315

[14] Liu, J., Lv, C. "Research Progress on Durability of Cellulose Fiber-Reinforced Cement-Based Composites", International Journal of Polymer Science, 2021(1), 1014531, 2021. https://doi.org/10.1155/2021/1014531

[15] Mohammed, L., Ansari, M. N. M., Pua, G., Jawaid, M., Islam, M. S. "A Review on Natural Fiber Reinforced Polymer Composite and Its Applications", International Journal of Polymer Science, 2015(1), 243947, 2015. https://doi.org/10.1155/2015/243947

[16] Sainz-Aja, J. A., Sanchez, M., Gonzalez, L., Tamayo, P., Garcia del Angel, G., Aghajanian, A., Diego, S., Thomas, C. "Recycled Polyethylene Fibres for Structural Concrete", Applied Sciences, 12(6), 2867, 2022. https://doi.org/10.3390/app12062867

[17] Shah, S. F. A., Chen, B., Oderji, S. Y., Haque, M. A., Ahmad, M. R. "Comparative study on the effect of fiber type and content on the performance of one-part alkali-activated mortar", Construction and Building Materials, 243, 118221, 2020. https://doi.org/10.1016/j.conbuildmat.2020.118221

[18] Wala, M. S., Mire, A., Dewangan, A. K. "Strength Characteristics of Glass Fiber Reinforced Concrete", International Journal of Engineering Research & Technology, 8(06), pp. 824–828, 2019. https://doi.org/10.17577/IJERTV8IS060537

[19] Zhang, P., Han, X., Zheng, Y., Wan, J., Hui, D. "Effect of PVA fiber on mechanical properties of fly ash-based geopolymer concrete", Reviews on Advanced Materials Science, 60(1), pp. 418–437, 2021. https://doi.org/10.1515/rams-2021-0039

[20] Prieto, T. G., Prieto, M. I., Leal, A., Ferrandez, D. "Mechanical Behavior of Carbon Fiber-Reinforced Concrete Structures After Structural Failure", Applied Sciences, 15(4), 1783, 2025. https://doi.org/10.3390/app15041783

[21] Džolan, A., Fischer, O., Jurišić, M. "Assessment of the development of strains/cracks in carbon-short-fiber-reinforced concrete (CSFRC) under static tensile loading using strain gauges and light-beam micrometer", Građevinski materijali i konstrukcije, 68(1), pp. 26–34, 2025. https://doi.org/10.5937/GRMK2500001D

[22] Džolan, A., Lauff, P., Fischer, O., Šunjić, G. "Influence of Concrete Shrinkage on the Behavior of Carbon Short-Fiber-Reinfoced Concrete (CSFRC) under Tension", Applied Sciences, 13(12), 7081, 2023. https://doi.org/10.3390/app13127081

[23] Fischer, O., Volkmer, D., Lauff, P., Hambach, M., Rutzen, M. "Zementgebundener kohlenstofffaserverstärkter Hochleistungswerkstoff (Carbonkurzfaserbeton)" (Cement-bonded, high-performance carbon-fiber-reinforced material (short-carbon-fiber concrete)), Fraunhofer IRB Verlag, 2019. ISBN 978-3-7388-0422-5 (in German)

[24] Lauff, P., Fischer, O. "Effizienter Ultrahochleistungsbeton mit innovativer trajektorienorientierter "Bewehrung"" (Efficient ultra-high-performance concrete with innovative trajectory-oriented "reinforcement"), Ce/Papers, 3(2), pp. 82–88. 2019. (in German) https://doi.org/10.1002/cepa.976

[25] Nerella, V. N., Ogura, H., Mechtcherine, V. "Incorporating reinforcement into digital concrete construction", presented at IASS Symposium 2018: Creativity in Structural Design, Boston, USA, 16–20 July 2018.

[26] Rutzen, M., Lauff, P., Niedermeier, R., Fischer, O., Raith, M., Grosse, C. U., Weiss, U., Peter, M. A., Volkmer, D. "Influence of fiber alignment on pseudoductility and microcracking in a cementitious carbon fiber composite material", Materials and Structures, 54(2), 58, 2021. https://doi.org/10.1617/s11527-021-01649-2

[27] Džolan, A., Fischer, O., Niedermeier, R. "Analyses of the fatigue behavior of carbon short-fiber-reinforced concrete (CSFRC) under tension and flexion", Construction and Building Materials, 453, 139058, 2024. https://doi.org/10.1016/j.conbuildmat.2024.139058

[28] Gao, H., Xia, Y. "Research on the dispersion of carbon fiber and recycled carbon fiber in cement-based materials: a review", Frontiers in Materials, 10, 1243392, 2023. https://doi.org/10.3389/fmats.2023.1243392

[29] Ghanem, S. Y., Bowling, J. "Mechanical Properties of Carbon-Fiber-Reinforced Concrete", Advances in Civil Engineering Materials, 8(3), pp. 224–234, 2019. https://doi.org/10.1520/ACEM20180089

[30] Bellary, V., Khartode, B., Shewale, M., Arangi, S. R., Shinde, N. "Experimental Investigation of Randomly Distributed Carbon Fibers in Concrete Beams", E3S Web of Conferences, 559, 04052, 2024. https://doi.org/10.1051/e3sconf/202455904052

[31] Zhang, J., Heath, A., Ball, R. J., Paine, K. "Effect of fibre loading on the microstructural, electrical, and mechanical properties of carbon fibre incorporated smart cement-based composites", Frontiers in Materials, 9, 1055796, 2022. https://doi.org/10.3389/fmats.2022.1055796

[32] Safiuddin, M., Abdel-Sayed, G., Hearn, N. "Absorption and Strength Properties of Short Carbon Fiber Reinforced Mortar Composite", Buildings, 11(7), 300, 2021. https://doi.org/10.3390/buildings11070300

[33] Ivorra, S., Garces, P., Catala, G., Andion, L. G., Zornoza, E. "Effect of silica fume particle size on mechanical properties of short carbon fiber reinforced concrete", Materials & Design, 31(3), pp. 1553–1558, 2010. https://doi.org/10.1016/j.matdes.2009.09.050

[34] Lauff, P., Fischer, O. "Damage indication by electrical resistivity measurement of carbon short fiber reinforced concrete in fatigue testing", In: Proceeding of the 2021 session of the 13th fib International PhD Symposium in Civil Engineering, Paris, France, 2021, pp. 258–265. ISBN 9782940643110